KeAi

CHINESE ROOTS
GLOBAL IMPACT

Contents lists available at ScienceDirect

Petroleum Science

journal homepage: www.keaipublishing.com/en/journals/petroleum-science



Original Paper

Influence of tectonic preservation conditions on the nanopore structure of shale reservoir: A case study of Wufeng-Longmaxi Formation shale in western Hubei area, south China



Meng Xiang ^a, Shang Xu ^{a, *}, Ya-Ru Wen ^b, Qi-Yang Gou ^c, Bing-Chang Liu ^a

- ^a National Key Laboratory of Deep Oil and Gas, China University of Petroleum (East China), Qingdao, 266580, Shandong, China
- ^b Hubei Key Laboratory of Resources and Eco-environment Geology, Hubei Geological Survey, Wuhan, 430034, Hubei, China
- ^c Key Laboratory of Tectonics and Petroleum Resources, Ministry of Education, China University of Geosciences, Wuhan, 430074, Hubei, China

ARTICLE INFO

Article history: Received 28 February 2023 Received in revised form 5 September 2023 Accepted 18 February 2024 Available online 21 February 2024

Edited by Jie Hao and Teng Zhu

Keywords:
Shale gas
Pore structure
Tectonic preservation conditions
Shale gas enrichment mechanism

ABSTRACT

Tectonism is one of the dominant factors affecting the shale pore structure. However, the control of shale pore structure by tectonic movements is still controversial, which limits the research progress of shale gas accumulation mechanism in the complex tectonic region of southern China. In this study, 34 samples were collected from two exploratory wells located in different tectonic locations. Diverse experiments, e.g., organic geochemistry, XRD analysis, FE-SEM, low-pressure gas adsorption, and high-pressure mercury intrusion, were conducted to fully characterize the shale reservoir. The TOC, Ro, and mineral composition of the shale samples between the two wells are similar, which reflects that the shale samples of the two wells have proximate pores-generating capacity and pores-supporting capacity. However, the pore characteristics of shale samples from two wells are significantly different. Compared with the stabilized zone shale, the porosity, pore volume, and specific surface area of the deformed zone shale were reduced by 60.61%, 64.85%, and 27.81%, respectively. Moreover, the macroscopic and fine pores were reduced by 54.01% and 84.95%, respectively. Fault activity and uplift denudation are not conducive to pore preservation, and the rigid basement of Huangling uplift can promote pore preservation. These three factors are important reasons for controlling the difference in pore structure between two wells shales. We established a conceptual model of shale pores evolution under different tectonic preservation conditions. This study is significant to clarify the scale of shale gas formation and enrichment in complex tectonic regions, and helps in the selection of shale sweet spots.

© 2024 The Authors. Publishing services by Elsevier B.V. on behalf of KeAi Communications Co. Ltd. This is an open access article under the CC BY-NC-ND license (http://creativecommons.org/licenses/by-nc-nd/

4.0/).

1. Introduction

Marine shale gas resources in South China have great potential. In recent years, significant breakthroughs have been made in the exploration and development of shale gas in Fuling, Weiyuan, Changning, and other areas in the Sichuan Basin. However, little attention has been paid to shale gas reservoirs in complex tectonic zones outside the basin. It is generally believed that shale formations in complex deformation zones have experienced multi-stage complex tectonic movements, and have the characteristics of low pressure coefficient, poor physical properties, complex preservation conditions, and poor gas content (He et al., 2016; Sun et al.,

* Corresponding author. E-mail address: xushang0222@163.com (S. Xu). 2020; Liu et al., 2023). The development difficulties are relatively large, and the economic benefit is not obvious. In fact, this kind of shale gas reservoir also has good resource potential, which can also be illustrated by the successful exploration of Well AY1 in Anchang syncline and Well Yiye 2 in Yichang slope zone. Moreover, such shale gas reservoirs are widely distributed in complex structural areas such as northeastern Chongqing, northern Guizhou and western Hubei, and have good resource potential (Zhai et al., 2017; Zhang et al., 2019). Therefore, it is necessary to systematically study the reservoir characteristics and enrichment controlling factors of shale gas reservoirs in complex tectonic zones.

Pores and fractures are important shale storage spaces, which significantly influences the storage and enrichment of shale gas (Ross and Bustin, 2009; Slatt and O'Brien, 2009; Chalmers et al., 2012; Milliken et al., 2013; Gou et al., 2019). Previous studies

have shown that lithofacies and tectonic preservation conditions are the main controlling factors for pore development (Mastalerz et al., 2013; Wu et al., 2016; Xu et al., 2020a). The pore characteristics of shale with different lithofacies usually have significant differences. Generally, the specific surface area and pore volume of micro-pores in organic-rich lithofacies shale are positively correlated with the TOC content, which is related to the formation of nanoscale OM pores by hydrocarbon generation (Xi et al., 2019: Wang and Guo, 2021). Milliken et al. (2012) found that siliceous shales have high specific surface area and pore volume due to the support of the rigid skeleton of brittle minerals. However, studies on the pore structure in some complex tectonic zone shales found that even if the organic matter types are the same, and the TOC content, Ro and mineral composition are similar, there are significant differences in their pore structure (Zhao et al., 2018; Hu et al., 2020; Xu et al., 2020b). These differences are mainly affected by tectonic preservation conditions and multi-stage tectonic deformations during burial and uplift (Liang et al., 2017; Ma et al., 2020; Gou et al., 2021a; Sun et al., 2023). Due to the complex pore structure and strong heterogeneity of shale reservoirs, understanding pore evolution associated with tectonic deformation remains controversial. Zhu et al. (2018) found that reservoirs can form more micron-sized fractures during tectonic activity, resulting in an increase in macropores, showing good reservoir properties and connectivity. In contrast, Xu et al. (2020b) concluded that tectonic activity would lead to the collapse and closure of most meso-pores and macro-pores in the shale, which is not conducive to the preservation of reservoir space. Therefore, the control of tectonism on the pore structure needs to be further clarified. In addition, it is necessary to better combine the differences of macro structural preservation to fully elucidate the control effect of tectonic action on the development and evolution of shale pores.

In this work, based on the study of two drillings within different tectonic units in western Hubei, the research objectives are as follows: (1) to clarify the difference in shale pore structure between the tectonic deformation area and tectonic stability area; (2) to explore the influence of tectonism on the development and evolution of organic-rich shale pores; (3) to establish the pore evolution model of shale under different tectonic preservation conditions.

2. Geological setting

The western Hubei region straddles two first-order tectonic units of the Yangtze platform and the Qinling-Dabie orogenic belt (Xu et al., 2021). The west is near to the Sichuan Basin, the east is close to the Jingmen-Dangyang syncline, the north is bounded by the Xiangguang fault, and the south is adjacent to the Jiangnan-Xuefeng Nappe uplift belt (Fig. 1). The study area has experienced the Caledonian, Hercynian, Indochinese, Yanshanian, and Himalayan tectonic movements, and the preservation conditions and reservoir characteristics are very complicated. There are many faults in the study area, which are mainly divided into NE-trending faults and NW-trending faults. The strata outcropping in the western Hubei region are complete, including the Proterozoic, Paleozoic, and Middle Cenozoic strata in order. In addition, three sets of organic-rich shales are developed in the area, namely, the Sinian Doushantuo Formation, Cambrian Niutitang Formation, and Upper Ordovician Wufeng Formation-Lower Silurian Longmaxi Formation (Fig. 2). The target layer of this study is the Wufeng-Longmaxi Formation shale. We sampled shale from two exploratory wells in the study area, which are located in the Huanling Uplift and Jianshi fault zones, respectively. The exploration depth of the target layer is less than 1000 m, which belongs to shallow shale formation. It is worth noting that the Huangling uplift, located

northwest of the Yichang area, has a the rigid granite basement, which has a certain anti-deformation effect on the overall structure of the region (Cai et al., 2021). Jianshi fault zone, located in the northern wing of the Huaguoping compound anticline of the Middle Yangtze plate, developed a series of northeastward folds and faults under the influence of multi-period tectonic movements (Zhou et al., 2021). Under the influence of the Jiangnan-Xuefeng uplift. Oianzhong uplift, and global sea level decline, the dark Wufeng-Longmaxi Formation shale in the study area is mainly formed in the occlusive basin, which is shallow-deep water shelf sedimentation. It is characterized by an anoxic reduction environment (Zhang et al., 2019), which is conducive to the deposition and preservation of OM. In addition, there are some fossils (radiolarian, graptolite, etc.) found in shale in western Hubei (Cai et al., 2022). It is noteworthy that the shale sedimentary environment of the two wells in the study area is similar, both of which are deep-water shelf sedimentary facies. The lithology is mainly black carbonaceous shale, siliceous shale, calcareous shale, and argillaceous shale.

3. Sample and methodology

3.1. Sample

This study collected 34 shale samples from the Wufeng-Longmaxi Formation in western Hubei (Fig. 3). Of these, 18 samples were from Well Y (located in the southeast wing of Huangling uplift, belonging to the tectonic stable area), and the sampling depth is 599.8—625.2 m. 16 samples were from Well M (located in the Jianshi fault zone, belonging to the tectonic deformation area), and the sampling depth is 854.4—899.7 m. The selected samples were tested by the total organic carbon (TOC) determination, porosity and permeability determination, X-ray diffraction (XRD) mineral analysis, Field emission scanning electron microscopy (FE-SEM), Low-pressure gas adsorption, and High-pressure mercury intrusion to analyze geochemical characteristics, mineral characteristics, and pore structure characteristics.

3.2. Mineralogical and organic geochemistry

The XRD technique is the most effective method to analyze and determine mineral components. According to the Chinese oil and gas industry standard SY/T5163-1995, the shale samples were crushed into powders larger than 200 mesh for XRD analysis. This experiment used a Bruker D8 Advance X-ray diffractometer for XRD analysis at 40 kV and 30 mA. The relative mineral content is determined by calculating the integral area under the curve of the main peak for the major minerals.

The CS844 analyzer was used to determine the total organic carbon content. Shale samples need to be pretreated before the experiment. Firstly, the samples were crushed into 100–200 mesh particles. Then, the powder samples were weighed to 100–200 mg and treated with superfluous dilute hydrochloric acid to remove the carbonate fraction. Finally, the samples were washed, dried, and put into the CS844 analyzer for high-temperature pyrolysis.

3.3. FE-SEM

FE-SEM can observe the morphological and structural characteristics of different types of pores. However, in the process of mechanical polishing of samples, it is easy to fracture some skeleton minerals, resulting in visual "false pores", which will affect the observation results. In this experiment, samples were cut without damage by the high-energy argon ion beam, which preserved the original morphology and structural characteristics of shale pores.

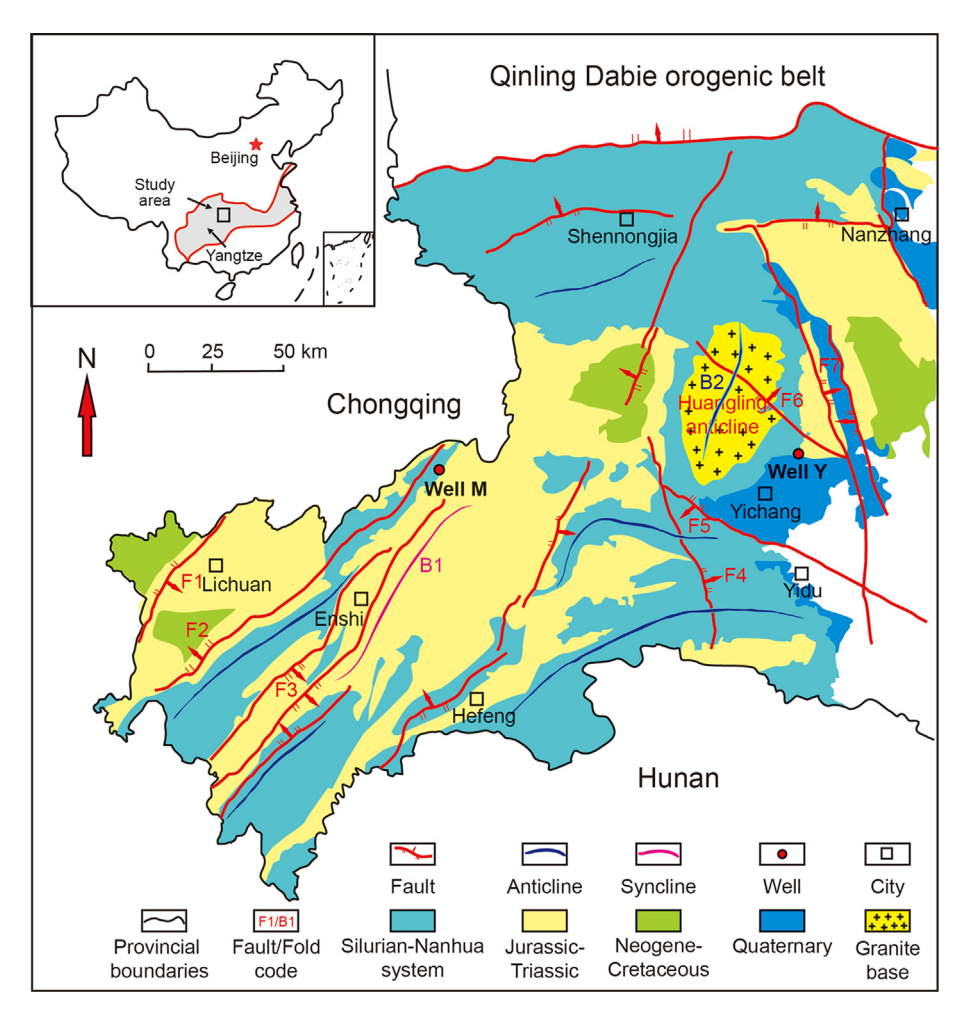


Fig. 1. Tectonic map of the western Hubei area, modified from Xu et al. (2021). (F1: Qiyueshan fault; F2: Jianshi-Pengshui fault; F3: Enshi-Qianjiang fault; F4: Xiannvshan fault; F5: Tianyangping fault; F6: Wuduhe fault; F7: Tongchenghe fault; B1: Huaguoping synclinorium; B2: Huangling anticline).

Then, the surface of the polished shale was coated with carbon to provide a conducting medium. Finally, we observed the morphological characteristics of shale pores with Zeiss MERLIN Compact 6174.

JMicroVision software can identify and analyze OM pores in FE-SEM images. The principle of this method is to identify and extract the pores by setting an appropriate gray threshold, and then carry on the statistical analysis of morphological characteristics of the identified pores. Through the analysis, we obtained some key parameters of OM pores, mainly including surface porosity (area of OM pores/area of OM), equivalent pore size, and roundness (short axis length/long axis length). Among them, the surface porosity can reflect the development degree of OM pores, the equivalent pore size can reflect the main distribution of OM pore diameter, and the roundness can reflect the regularity of OM pores.

3.4. Low-pressure gas adsorption

Low-pressure gas adsorption (CO_2 adsorption and N_2 adsorption) is an important method to quantitatively characterize the microscopic pore structure of shale reservoirs. Generally, we measure the adsorbed amount of carbon dioxide or nitrogen under different pressure conditions. We then choose the relevant calculation model to calculate the pore volume, specific surface area, and pore size distribution. The ASAP 2460 analyzer was used for the low-pressure gas adsorption test. Before the experiment, 80-100

mesh shale powder samples were dried for 12 h at 110 °C in the degassing chamber to eliminate free water and impurity gas in the samples. Then, the degassing samples were placed in CO_2 at 0 °C and N_2 at -196 °C, respectively, to obtain the Isothermal adsorption curve. Finally, Density Functional Theory (DFT) model and Barrett Joyner Halenda (BJH) model were used to calculate pore volume and pore size distribution of shale pores, Brunauer Emmett Teller (BET) model was used to calculate the specific surface area.

3.5. High-pressure mercury intrusion

High-pressure mercury intrusion is widely used to analyze the pore size distribution of porous materials. The instrument used in this study is Micromeritics Auto Pore IV 9520. Before the experiment, cube samples with a side length of 1 cm were prepared and placed in a 110 °C oven for 24 h to eliminate the influence of moisture. And then, the samples were sealed in an expansion agent and pressurized to inject mercury. Finally, the mercury intake under different pressures was detected by sensors. Based on the Washburn equation, the pore radius corresponding to each mercury injection pressure can be calculated. Then, the pore volume corresponding to each pore radius can be obtained (Jiao et al., 2020). The Washburn equation could be described as follows:

$$p = 2\sigma \cos\theta/r \tag{1}$$

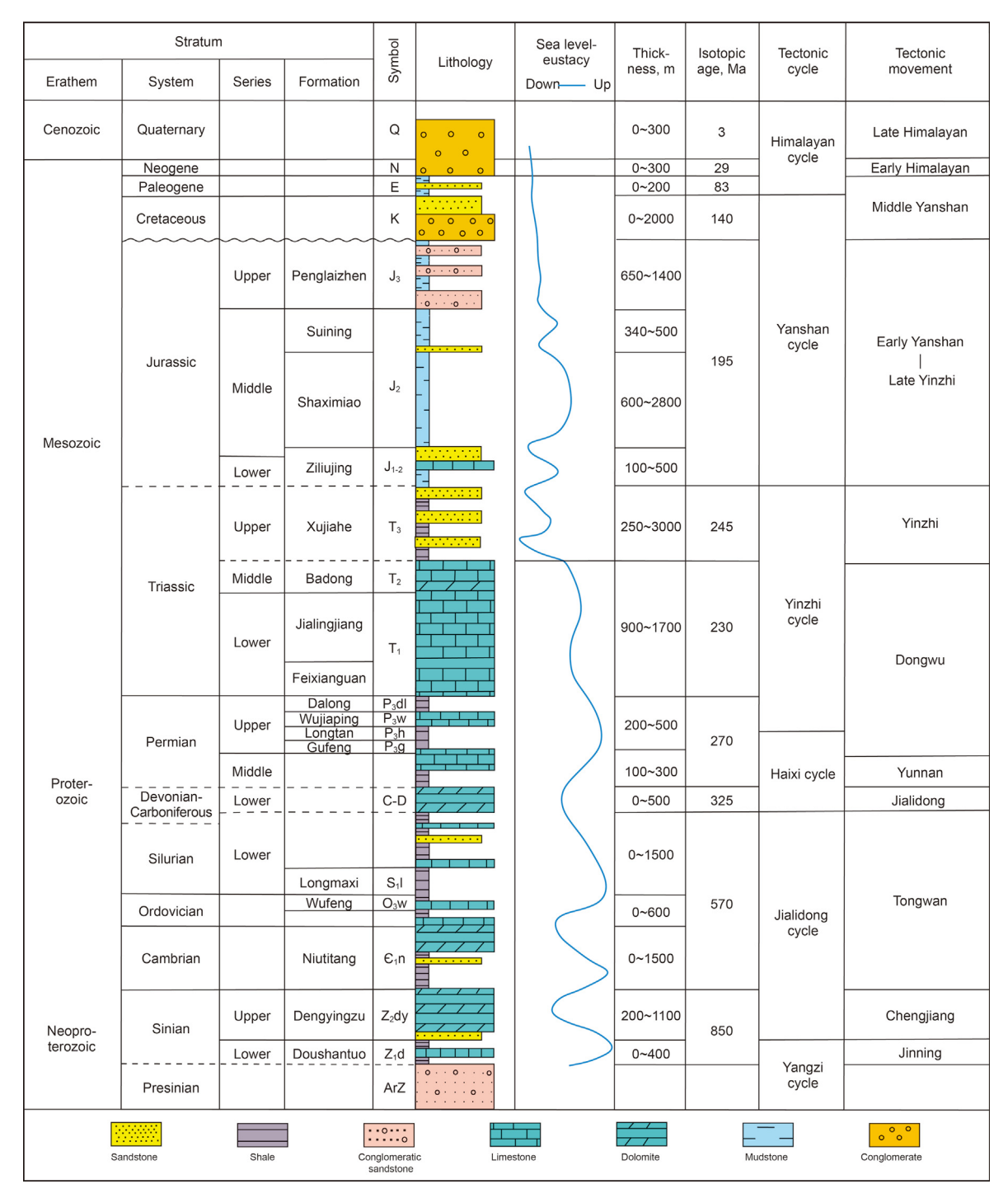


Fig. 2. Stratigraphic column of the western Hubei area, modified from Zhang et al. (2019).

where p is the mercury injection pressure, σ is the surface tension of mercury (σ is 0.4842 N/m), θ is the contact angle between mercury and mercury (θ is 130°), and r is the pore radius.

4. Results

4.1. Mineral composition, shale lithofacies, and TOC

As seen in Fig. 4, the shale core of Well Y is dark gray, and the core is relatively complete and continuous. Most shale samples

have original parallel lamination, and some weakly deformed shales have detachment fault mirrors. In contrast, the shale core from Well M is light gray with a high degree of core fracture, indicating that deep fracture zones may be encountered during drilling. Furthermore, the deformed shale has more medium to high angle fractures and detachment fault mirrors. The XRD results (Fig. 5a) showed that the mineral composition of shale in Well Y is mainly composed of quartz and clay, accounting for 47% and 43%, respectively. The content of feldspar, calcite, and pyrite is limited. According to the ternary diagram of felsic minerals, carbonate

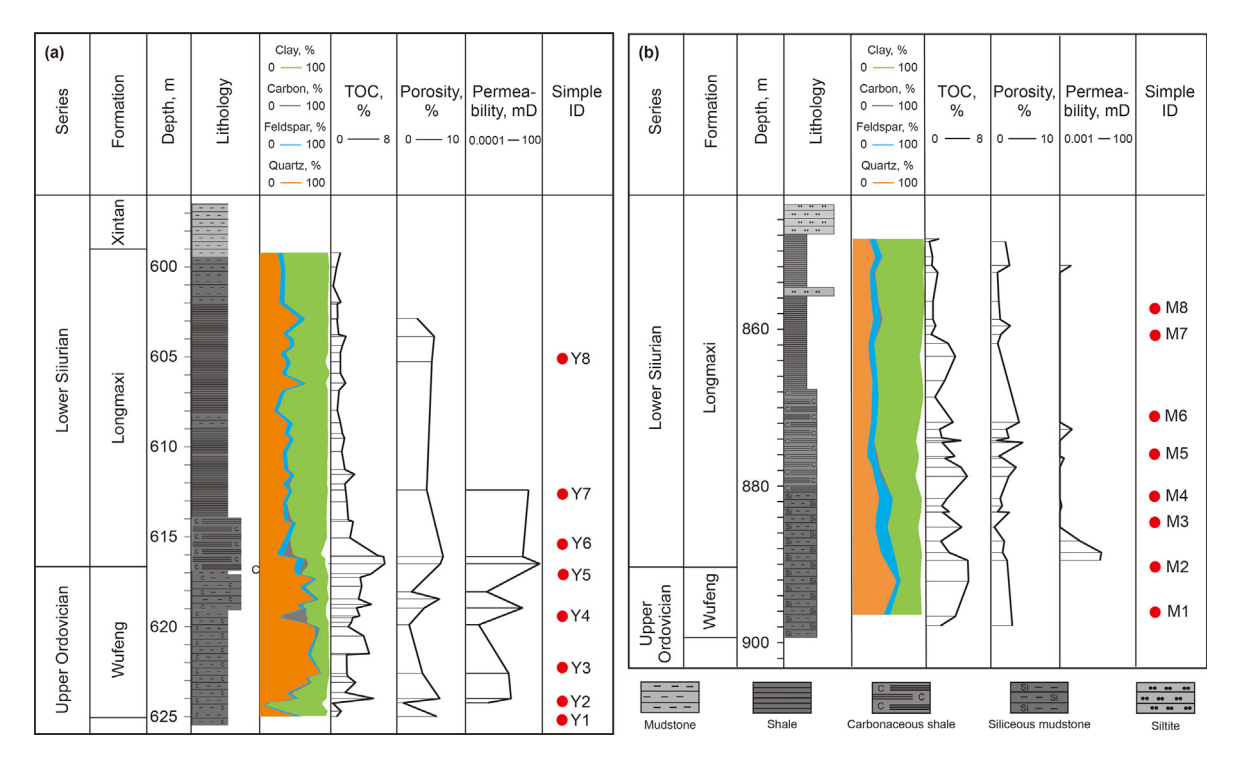


Fig. 3. Lithofacies, mineral compositions, TOC, Porosity, and Permeability in the Well Y (a) and Well M (b) of the western Hubei area.

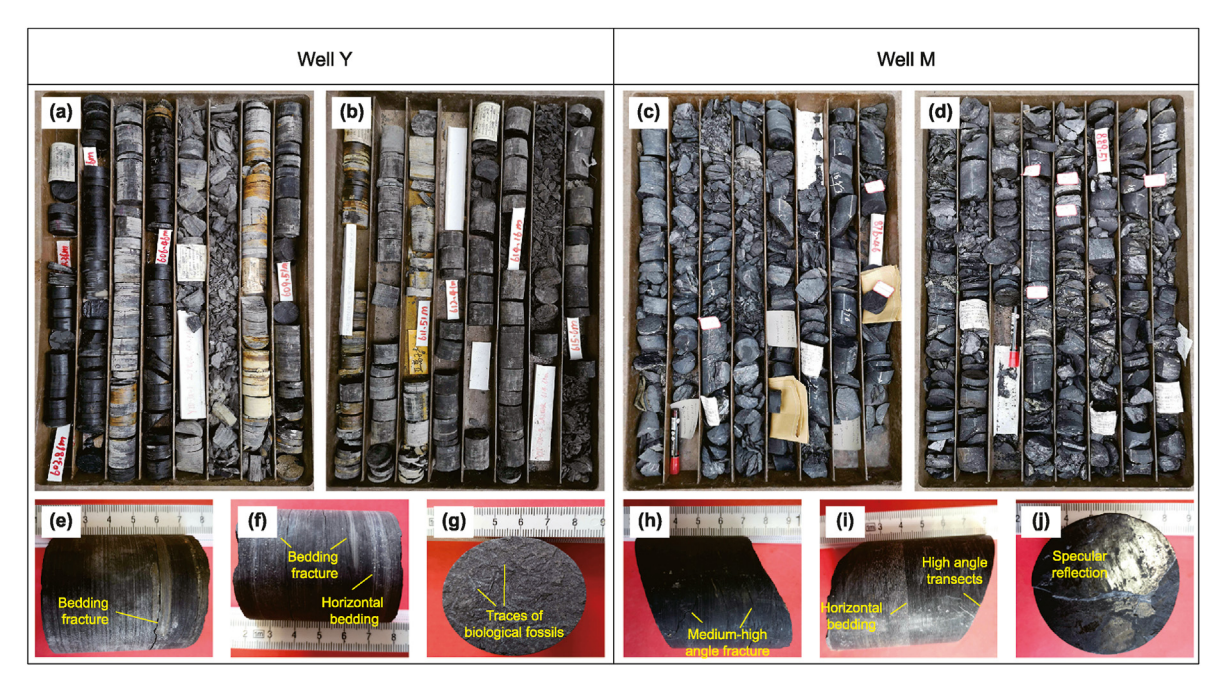


Fig. 4. Characteristics of Shale cores from Wufeng-Longmaxi Formation shale reservoirs in the western Hubei area.

minerals, and clay minerals (Fig. 5b), we noted that the lithofacies of Wufeng-Longmaxi Formation shale in Well Y are mainly silicarich argillaceous shale lithofacies (CM-1) and clay-rich siliceous shale lithofacies (S-3). Only a few samples are mixed lithofacies (M-2) and siliceous shale lithofacies (S). Similarly, the mineralogical composition of the shale in Well M is dominated by clay and quartz, 51% and 30%, respectively, and the lithofacies are also dominated by CM-1 and S-3. Compared with the shale of Wufeng-Longmaxi Formation in Jiaoshiba area, the shales in both areas were formed

in a closed and retained deep water reduction environment, and the average TOC content of the shales is higher (more than 2%). The mineral composition is mainly siliceous and clay minerals, and the lithofacies is mainly CM-1 and S-3 (Xu et al., 2020b). Therefore, it is considered that the shale samples in western Hubei have similar material composition to the shale in Jiaoshiba area, and also have typical shale characteristics in complex tectonic areas. As shown in Fig. 6a, The TOC of Well Y shale ranges from 0.7% to 6.29%, with an average value of 2.30%. The main distribution range is 0–3%,

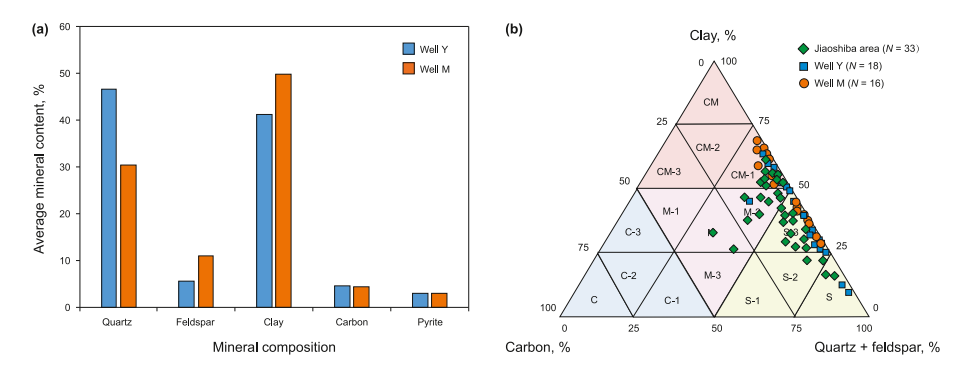


Fig. 5. Mineral composition (a) and lithofacies distribution (b) of the Wufeng-Longmaxi shale samples in the western Hubei area.

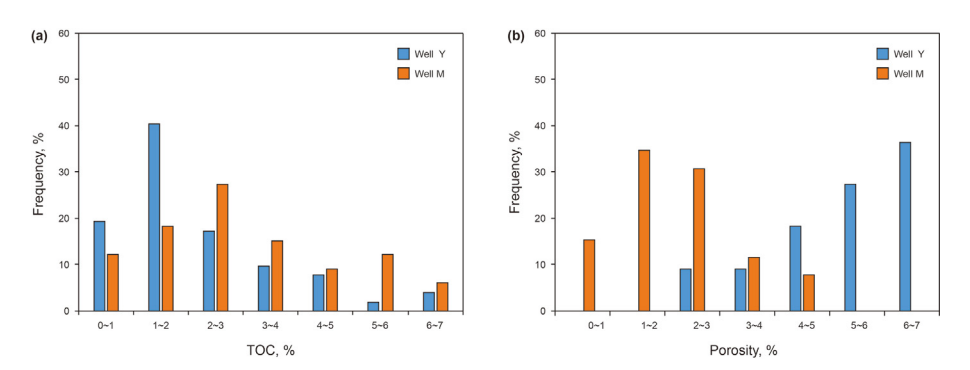


Fig. 6. The distribution of TOC (a) and Porosity (b) in shales from Well Y and Well M in the western Hubei area.

accounting for 73.91%. However, the TOC of Well M shales ranges from 0.81% to 6.20%, with an average value of 2.93%. The main distribution ranges from 1% to 4%, accounting for 60.61%.

4.2. Shale porosity

Fig. 6b shows the porosity distribution of shale. The range of shale porosity in well Y is 2.94%—6.77%, with a mean of 5.18%, and the main distribution range is 4%—7%, accounting for 64.28%. By contrast, Well M shales exhibit a lower porosity, ranging from 0.52% to 4.62%, with a mean of 2.04%, and the main distribution range is 0—3%, accounting for 85.18%. We noted that the shales in both wells have a similar mineral composition. The average TOC content of the shale in Well Y is lower than that of Well M. However, Well Y shale porosity is significantly higher than Well M. Therefore, we analyze the correlation between shale composition and porosity. The result (Fig. 7a) shows a good positive correlation between TOC and porosity in Well Y shales. However, there is no apparent correlation between TOC and porosity in Well M shales (Fig. 7d). Meanwhile, the correlation between shale porosity and mineral composition is not apparent in the two wells (Fig. 7b, c, e, and f).

4.3. Pore structure from FE-SEM

Fig. 8 shows the FE-SEM images of organic matter pores in the shales of two wells. OM pores are the most developed in the Wufeng-Longmaxi Formation shale of Well Y. A large number of OM pores can be observed under the microscope, with the pore size ranging from 50 nm to 100 nm. The OM pores are mainly elliptic, spongy, and bubbly. It is noteworthy that some large-aperture OM pores were deformed and showed a slit shape. Interparticle (interP) pores and intraparticle (intraP) pores are also relatively developed pore types in shales. The pore size is generally larger than 200 nm

and the shape is usually irregular. Under the microscope, a few microfractures can also be observed, mostly on the nanometer to micron scale. They are mainly structural fractures, OM shrinkage, and clay interlayer fractures. However, the development of OM pores in Well M is significantly reduced, and most OM pores are disconnected. The pore size is generally less than 60 nm, and the pore morphology is mostly flat elliptic, and irregular. The development of inorganic pores and micro-fractures in Well M is similar to that in Well Y.

By using [MicroVision software, 96 electron microscopic photos of 8 shale samples were used to conduct statistics and analysis on the pore structure parameters. The results of the OM surface porosity (Fig. 9a and d) show that the peak OM surface porosity of Well Y shales is mainly distributed from 12% to 16% (mean 12.6%), while that of Well M shales is mainly distributed from 0 to 4% (mean 6.4%). The OM surface porosity of Well Y shales is significantly higher than that of Well M shales, which is consistent with the results of porosity tests. The pore size distribution statistics (Fig. 9b and e) shows that the equivalent size of OM pores in Well Y mainly ranges from 10 nm to 70 nm, while that in Well M primarily ranges from 10 nm to 40 nm. The pore size of the shales in Well Y is larger than that of the shales in Well M. The result of roundness statistic (Fig. 9c and f) shows that the roundness distributions of both Well shales are similar, and the roundness of Well Y shales is slightly higher than that of Well M shales.

4.4. Pore structure

4.4.1. Pore structure from CO₂ adsorption

The CO_2 adsorption isotherms are shown in Fig. 10a and b. As the relative pressure (p/p_0) increases from 0 to 0.03, the CO_2 adsorption isotherms of the shale samples increase rapidly in both the stable and deformed zones. This adsorption curve feature is consistent

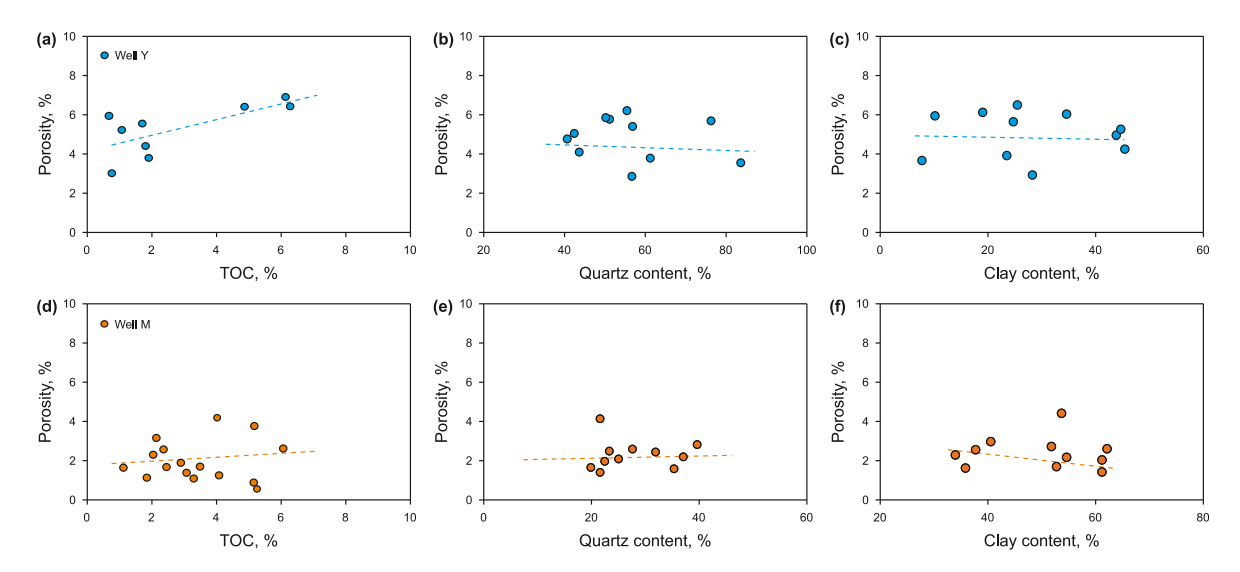


Fig. 7. The relationships between porosity and TOC, Quartz content, and Clay content of the Wufeng-Longmaxi shale samples in the western Hubei area.

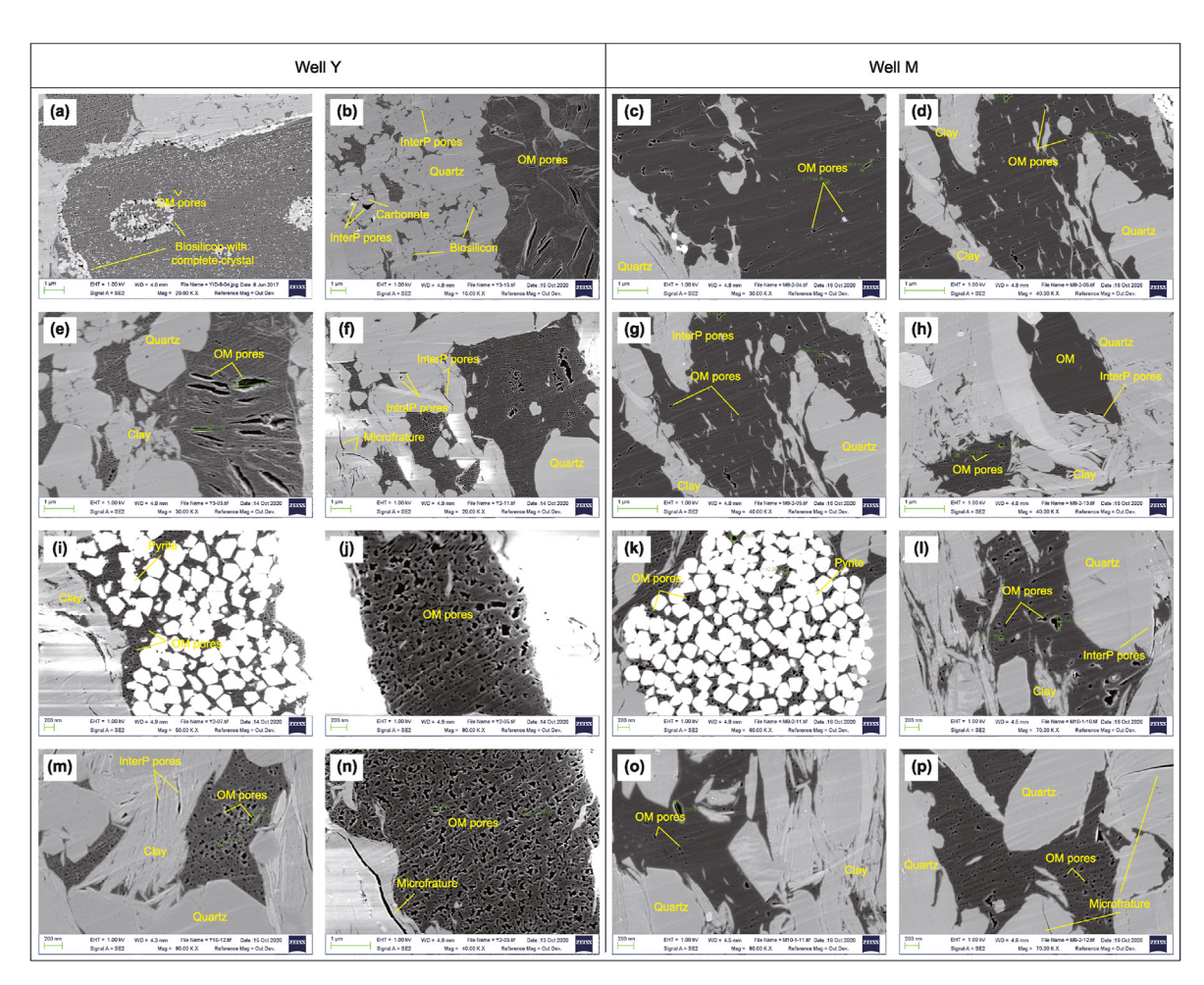


Fig. 8. FE-SEM images of the Wufeng-Longmaxi Formation shale samples from Well Y and Well M in the western Hubei area.

with the type I physical adsorption model proposed by IUPAC, indicating a high degree of micro-pores development in the shale samples. The maximum adsorption volume of shale samples in Well Y ranges from 0.57 cm³/g to 2.04 cm³/g, with a mean of 1.26 cm³/g. We noticed that the shales in Well M exhibit a similar

maximum adsorbed volume, varying from 0.94 cm³/g to 2.08 cm³/g, with a mean of 1.29 cm³/g. Based on the DFT model, the micropores volume of shales in Well Y is calculated to be $1.8\times10^{-3}-7.1\times10^{-3}$ cm³/g (mean 4.07 \times 10^{-3} cm³/g), while that of shales in Well M is 2.3 \times $10^{-3}-5.3$ \times 10^{-3} cm³/g (mean

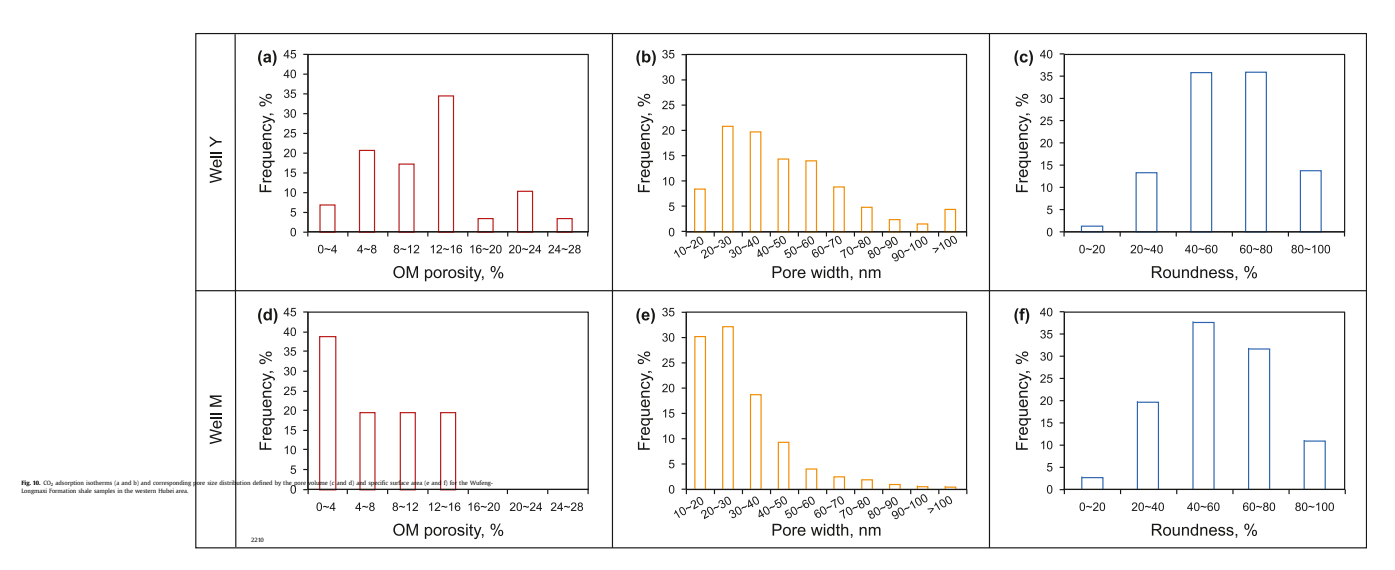
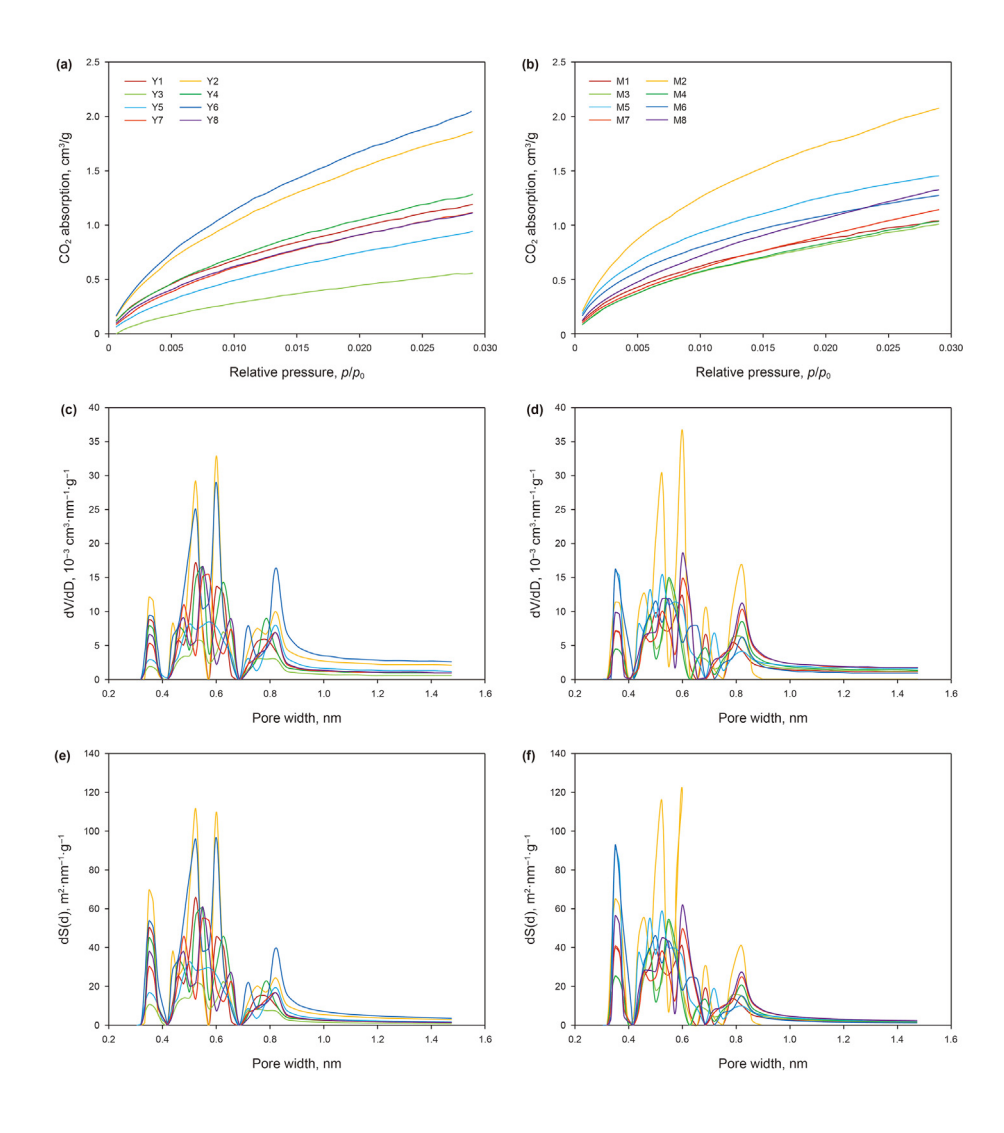


Fig. 9. The distribution of OM surface porosity (a and d), pore width (b and e), and roundness (c and f) of OM pores obtained from FE-SEM images.



 $3.81\times10^{-3}~cm^3/g).$ As shown in Fig. 10c–f, the pore size distribution curves of shale samples in both wells have multiple peaks in

the range of 0.35-0.8 nm, indicating that the pore volume and specific surface area of shale samples are mainly provided by pores

with the size of 0.35-0.8 nm. The above comparison shows that the micro-pore structure characteristics of shales in both wells are similar.

4.4.2. Pore structure from N_2 adsorption

Fig. 11a and b shows the N2 sorption-desorption isotherms of various shale samples. According to the IUPAC classification, the types of capillary hysteresis loops are mainly the mixture of H2 (ink bottle type) and H4 (slit type). Meanwhile, we also noticed that the primary hysteresis loop type of shales in Well Y is H2 type, while that of shales in Well M is mainly H4 type. It means that the shales in Well Y have a larger storage space, which is more conducive to gas adsorption and storage. In addition, the maximum adsorption volume of shales in Well Y ranges from 7.73 cm³/g to 20.04 cm³/g, with a mean of 13.02 cm³/g. By contrast, the shales in Well M exhibit a lower maximum N₂ adsorption volume, which varies from $5.43 \text{ cm}^3/\text{g}$ to $8.89 \text{ cm}^3/\text{g}$, with a mean of $7.11 \text{ cm}^3/\text{g}$. According to the BJH model, the volume of meso-pores in Well Y shales is $8.4 \times 10^{-3} - 19.8 \times 10^{-3}$ cm³/g (mean 13.7×10^{-3} cm³/g), while that of Well M is $4.8 \times 10^{-3} - 8.3 \times 10^{-3}$ cm³/g (mean 6.3×10^{-3} cm³/g). As shown in Fig. 11c–f, the pore size distribution curves of shales show multiple peaks in the range of 1.0-2.0 nm. In addition, we further noticed that the average peak values of pore volume and specific surface area change rate

 $12.21\times 10^{-3}~cm^3~nm^{-1}\cdot g^{-1}$ and 57.13 $m^2~nm^{-1}\cdot g^{-1}$, while that of Well M shales are 5.64 $\times~10^{-3}~cm^3~nm^{-1}\cdot g^{-1}$ and $20.25~m^2~nm^{-1}\cdot g^{-1}$. The above results suggest that the pore volume and specific surface area of the Well Y shales are significantly higher than those of Well M.

4.4.3. Pore structure from high-pressure mercury intrusion

As shown in Fig. 12a and b, the capillary curves of both wells have similar shapes, and the mercury saturation curve increases significantly when the mercury injection capillary pressure is 30-110 MPa. In addition, the average cumulative mercury saturation of Well Y shales is 20.68%, while that of Well M is 11.80%. It also can be seen from Fig. 12c and d that the pore size distribution of Well Y shales exhibits a multi-peak distribution, with four apparent peaks at 10 nm, 50 nm, 600 nm, and 2 µm. However, there are only two apparent peaks in Well M shales at 10 nm and 1 µm. Moreover, the peak pore volume of shales in Well Y is much higher than that in Well M. Comparing the pore volume of shales in both wells, the pore volume of Well Y shales is 0.0249-0.0932 cm³/g (average $0.0471 \text{ cm}^3/\text{g}$), while that of Well M is $0.0108-0.0295 \text{ cm}^3/\text{g}$ (average 0.0155 cm³/g). The above results indicate that the development degree of meso-pores and macro-pores in the shale of Well Y is significantly better than that of the shale of Well M.

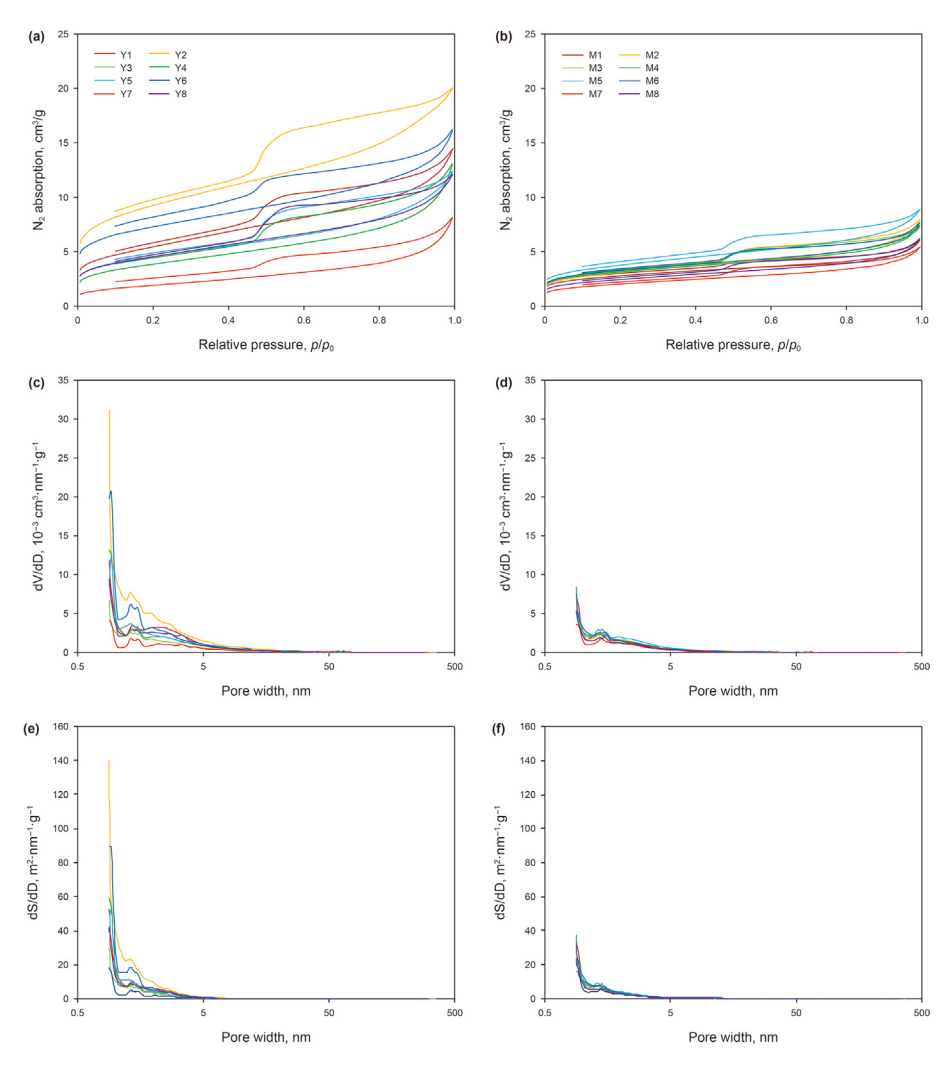


Fig. 11. N₂ adsorption-desorption isotherms (a and b) and corresponding pore size distribution defined by the pore volume (c and d) and specific surface area (e and f) for the Wufeng-Longmaxi Formation shale samples in the western Hubei area.

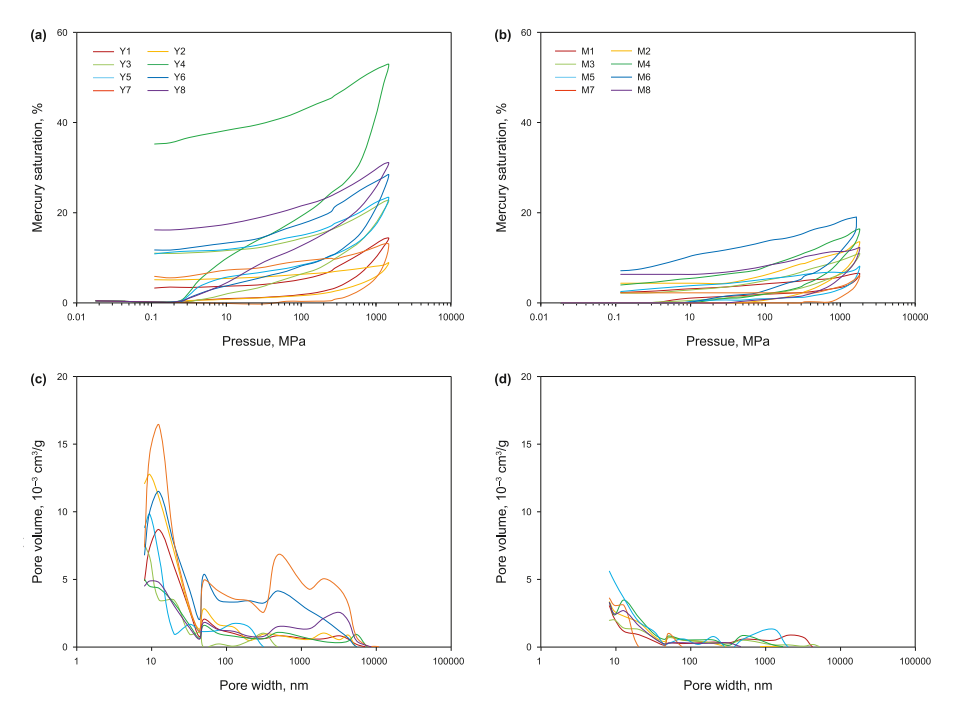


Fig. 12. Capillary pressure curve (a and b) and corresponding pore size distribution (c and d) for the Wufeng-Longmaxi Formation shale samples in the western Hubei area.

4.4.4. Pore structure from full-scale pores characterization

In order to accurately and comprehensively characterize the pore structure characteristics of shale reservoir, we combined CO₂ adsorption (used to characterize micro-pores), N2 adsorption (used to characterize meso-pores), and high-pressure mercury intrusion (used to characterize macro-pores) to conduct full-scale pore characterization. As shown in Fig. 13, the pore size distribution of Well Y shales shows a multi-peaked distribution with obvious peaks at 0.6 nm, 10 nm, and 600 nm, with peak sizes of 0.39 cm 3 /g, 0.72 cm³/g, and 0.24 cm³/g, respectively. By contrast, the pore size distribution of Well M shales shows a double-peak distribution at 0.6 nm and 10 nm, with peak sizes of 0.35 cm³/g and 0.43 cm³/g, respectively. Fig. 14 and Table 1 show the total pore volume and specific surface area of the shales in the two wells. The average total pore volume and specific surface area of Well Y shales are 0.039 cm³/g and 28.47 m²/g, while that of shales in Well M is 0.013 cm³/g and 18.76 m²/g. In addition, it is noticed that mesopores and macro-pores are the main contributors to the pore volume of Well Y shales, accounting for 36.82% and 47.61%, respectively. However, the pore volume of Well M shales is mainly contributed by micro-pores and meso-pores, accounting for 32.56% and 46.89%, respectively. Moreover, the micro-pores contribute significantly to the total specific surface area of shales in both wells. By comparing the pore volume, specific surface area, and pore size distribution of shales in both wells, it is found that there is little difference in the micro-pores characteristics of shales in both wells. However, the structural characteristics of meso-pores and macro-pores of Well Y shales have significant advantages.

5. Discussion

5.1. The pores-generating capacity of OM and the supporting capacity of mineral

OM is the material basis for the formation of OM pores in shale (Wang et al., 2014, 2021b; Teng et al., 2022). Generally, thermal maturity is an essential factor determining the hydrocarbongeneration evolution process of OM (Chen and Xiao, 2014; Zhang et al., 2020; Gao et al., 2020). These two factors are essential factors affecting the original quality of shale reservoirs (Cao et al., 2018; Xu et al., 2020b; Si et al., 2022). The average TOC content of shales in both wells is greater than 2%, which shows good

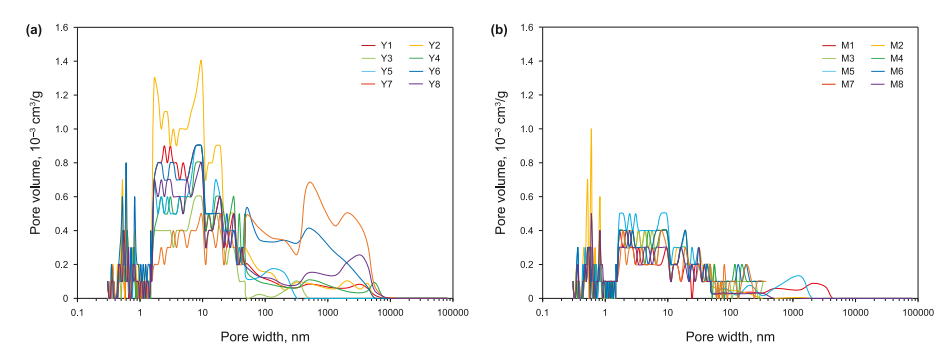


Fig. 13. Full-scale pore size distribution obtained from combination of CO₂ adsorption, N₂ adsorption, and high-pressure mercury intrusion for the Wufeng-Longmaxi Formation shale samples in the western Hubei area.

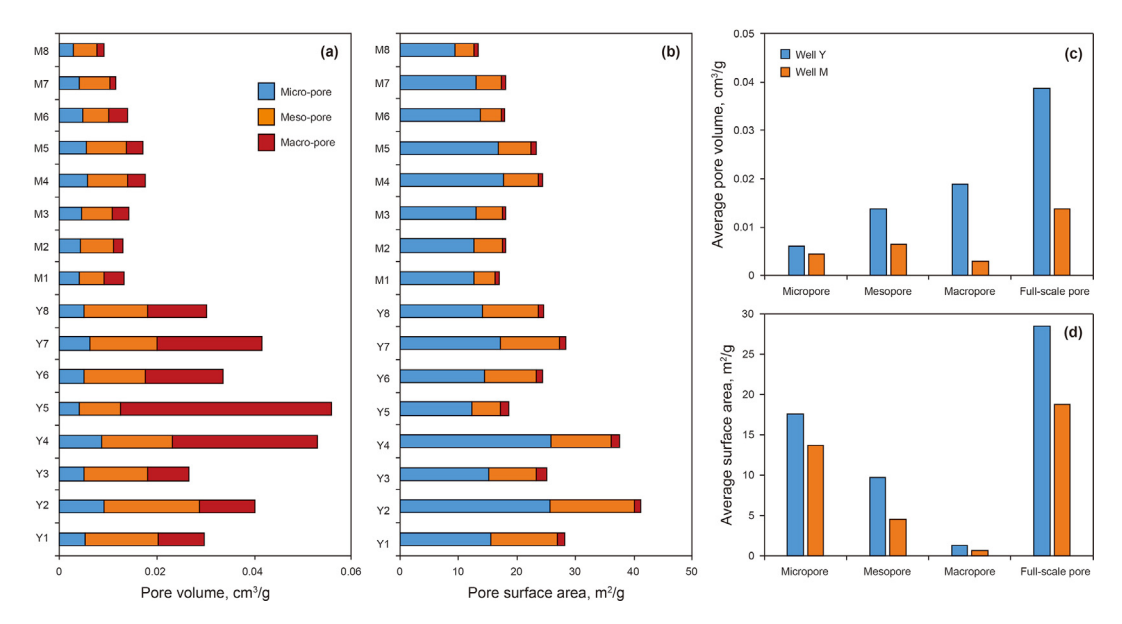


Fig. 14. Distribution of pore volume (a and c) and pore surface area (b and d) for the Wufeng-Longmaxi Formation shale in the western Hubei area.

Table 1Summary of fundamental pore structure parameters of the measured shale samples from the Wufeng-Longmaxi Formation in the western Hubei area.

Sample ID	Pore volume, 10^{-3} cm 3 /g				Specific surface area, m ² /g			
	Micro-pores	Meso-pores	Macro-pores	Total	Micro-pores	Meso-pores	Macro-pores	Total
Y1	0.0053	0.0149	0.0094	0.0296	15.58	11.27	1.34	28.19
Y2	0.009	0.0198	0.0113	0.0401	25.66	14.42	1.00	41.08
Y3	0.0049	0.0131	0.0085	0.0265	15.19	8.05	1.79	25.03
Y4	0.0087	0.0144	0.0297	0.0528	25.77	10.39	1.39	37.55
Y5	0.0040	0.0084	0.0433	0.0557	12.39	4.87	1.29	18.56
Y6	0.0049	0.0126	0.0159	0.0334	14.41	8.93	1.08	24.42
Y7	0.0062	0.0137	0.0215	0.0414	17.18	10.05	1.04	28.27
Y8	0.0050	0.0130	0.0122	0.0302	14.21	9.38	1.02	24.61
M1	0.0041	0.0050	0.0042	0.0133	12.68	3.67	0.60	16.96
M2	0.0043	0.0067	0.0020	0.0130	12.67	4.88	0.56	18.12
M3	0.0045	0.0064	0.0032	0.0141	13.08	4.50	0.19	17.78
M4	0.0056	0.0083	0.0035	0.0174	17.65	6.06	0.76	24.47
M5	0.0054	0.0082	0.0036	0.0172	16.76	5.73	0.91	23.40
M6	0.0048	0.0052	0.0039	0.0139	13.84	3.55	0.55	17.93
M7	0.0041	0.0063	0.0010	0.0114	13.05	4.33	0.64	18.03
M8	0.0028	0.0048	0.0015	0.0091	9.50	3.22	0.64	13.36

hydrocarbon-generating potential (Furmann et al., 2014). In addition, the average thermal maturity of shales in Well Y and Well M is 2.05% and 2.56%, which are both in the over-mature thermal evolution stage. In this case, the previously generated liquid hydrocarbons and bitumen are further cracked at high temperatures to form dry gas, thus forming more OM pores (Chen and Xiao, 2014; Wang et al., 2021b). Therefore, it can be considered that the shales of both wells have good original pores-generating capacity. However, the results of pore structure characterisation indicate that there is a significant difference in the preservation of organic matter pores in the shales of the two wells. This is consistent with the results of the previous correlation analysis between porosity and TOC. The OM pores in Well Y shales are well preserved, and the contribution of OM pores to porosity is high. However, the OM pores in Well M shales are poorly preserved, and the contribution of OM pores to porosity is limited.

The mineral composition is an important reason to control the preservation of OM pores. Especially, brittle minerals, e.g., quartz, feldspar, possess high elastic modulus, low Poisson's ratio, and high compressive strength (Yasin et al., 2021). In such cases, they can

resist compaction of OM pores during multiple geological tectonic movements (Wang, 2020; Yang et al., 2022). As seen in Fig. 5, the shale samples of the two wells have similar mineral composition, and the brittle mineral content of the shales of Well Y and Well M is 48.7% and 56.8%, respectively. Notably, as shown in Fig. 8, some bio silicon with a complete crystal shape also developed in the two wells shales, and this siliceous mineral framework plays an effective role in resisting pressure and preserving OM pores (Dong et al., 2019). In conclusion, the shales of both wells have good poresupporting capability. Combined with the previous analysis, there is no significant correlation between shale porosity and mineral content in both wells. It shows that the mineral content is not the main factor controlling the difference of OM pore preservation.

5.2. Effect of tectonic preservation on shale pores

Western Hubei has experienced Caledonian, Hercynian, Indosinian, and Himalayan tectonic movements, resulting in complicated structures in this area. Accordingly, the tectonic preservation condition is critical for the preservation of OM pores. In this

research, we will discuss the influence of tectonic preservation conditions on the pore structure of shale from three aspects: fault activity, uplift denudation, and Huangling uplift.

5.2.1. Destruction of pores by fault activity

Fault activity is the process of rock fracture caused by stress release accumulated by tectonic movement, which is often accompanied by cracks (Hu et al., 2014; Shi et al., 2022). The development of many fractures will destroy the sealing properties of the shale system, reduce shale formation pressure, and then affect the structural characteristics of pores. In addition, the closer the shale reservoir is to the fault zone, the stronger the tectonic stress is and the higher the degree of tectonic deformation in the shale (Shi et al., 2022; Liu et al., 2023). As shown in Fig. 1, Well M is 3.7 km from the Jianshi-Pengshui fault, and Well Y is 6.5 km from the Wuduhe fault. Accordingly, it is noted that the core of Well M, which is close to the fault zone, is seriously fractured, and many medium-high angle shear fractures have developed. These fractures have the characteristics of a straight section, large dip angle, far extension, and no filling. Some large-scale shear fractures can even penetrate multiple formations and communicate multiple fractures to form a complex fracture network system. This developed fracture network easily becomes a favorable channel for shale gas to escape, which is not conducive to shale gas enrichment (Hu et al., 2014). The core of Well Y, far from the fault zone, is well preserved, and the fracture development type is mainly low-angle slip fracture along the bedding. This kind of crack angle is small, generally horizontal or low angle (5°-10°). Most of these are medium and small closed fractures, which will not cause much shale gas to escape (Wang et al., 2021a). Combining the results of the pore structure characterization of the shale from the two wells, we believe that a large amount of shale gas escapes from the shale reservoir in well M along the fracture channels, resulting in poor gas content in the reservoir and low formation pressure. Therefore, the OM pores that lose the support of overpressure fluid will collapse and close under compaction (Zhao et al., 2018; Xu et al., 2020b; Gou et al., 2021a). Therefore, we believe that fault activity is not conducive to preserving shale pores.

5.2.2. Destruction of pores by uplift denudation

Intensive uplift and denudation lead to changes in the stressstrain characteristics, temperature-pressure environment, and physical characteristics of shale reservoirs, which affect the gasbearing property and its preservation condition (Wei et al., 2019; Guo et al., 2022). With the uplift of different degrees, the shallow strata will also have different denudation processes, exposing the strata of different ages. The formation outcropping in the study area shows that the outcropping layer of Well M is older than that of Well Y, indicating that shale formation in Well M is more affected by uplift and denudation. Similarly, influenced by the difference in formation fracture development during uplift, the shales of the two wells show different pore structures and shale gas enrichment characteristics. The reasons for fracture formation are as follows: (1) The uplift and denudation of strata may lead to the imbalance of the internal and external pressure of shale, resulting in brittle fracture or reopening of fractures in the closed state of shale (Hu et al., 2014; Liu et al., 2020). (2) The transformation from plasticity to brittleness occurs in the uplifting process of shale (Yuan et al., 2017), leading to the brittle fracture of shale easily. The result is that when a large amount of shale gas escapes to the surface along these fractures, OM pores will collapse and close due to insufficient fluid pressure to support pore morphology, resulting in a significant decrease in shale pore volume and specific surface area (Zhao et al., 2018; Gou et al., 2021b; Yang et al., 2022). Therefore, it can be considered that uplift denudation has seriously damaged the preservation of OM pores.

5.2.3. Protection of pores by Huangling uplift

Compared to marine shale in most complex structural areas in southern China, organic-rich shales in the Yichang area of western Hubei have the advantages of lower thermal evolution, better reservoir capacity, and higher gas content, which are mainly related to the rigid basement of the Huangling uplift (Zhang et al., 2019). The Huangling uplift developed a hard and thick granite basement, which separated the heat exchange between the strata above the basement and the deep fluid (Ge et al., 2013). Moreover, Bao et al. (2018) noted that the geothermal gradient of the sedimentary strata around the Huangling uplift is low, only 2.17 °C/100 m. Therefore, it is suggested that the rigid basement significantly influences the thermal evolution of OM. In this research, the average thermal maturity of Wufeng-Longmaxi Formation shale in Well Y and Well M in the study area is 2.05% and 2.56%, respectively. We noticed that the thermal maturity of shale in Well Y, located in the southeast wing of Huangling uplift, is lower than that in Well M, which also confirms the thermal insulation effect of the rigid basement of the Huangling uplift. Due to the heat insulation effect of its rigid basement, the source rocks around the Huangling uplift have lower thermal maturity (Chen et al., 2020; Zhang et al., 2021). When the thermal maturity is too high (Ro>3.5%), OM will carbonize, resulting in a large reduction in OM pores. Therefore, it can be considered that the OM of Well Y shale is in a favorable thermal evolution stage under the heat insulation action of the rigid basement of the Huangling uplift.

Although the study area has undergone multiple periods of tectonic movement, the basement of the Huangling uplift is mainly composed of Proterozoic granite with uniform mechanical properties. In the process of tectonism, the Huangling uplift is a relatively complete structural unit, so it is less reformed by faults and folds (Chen et al., 2020). In addition, the rigid basement of the Huangling uplift has the advantages of early formation, wide distribution, late uplift, and strong deformation resistance, which ensures the structural stability of the ancient shale layer above the basement uplift (Zhang et al., 2019; Chen et al., 2020). Well Y is located in the Yichang slope belt on the southeast wing of the Huangling ancient uplift, and its rigid granite basement resists the destruction of pores by the tectonic movement to some extent (Bao et al., 2018; Zhai et al., 2019; Zhang et al., 2021). Although faults such as the Wuduhe and Tianyangping faults are developed around the Huangling uplift, the core of the Wufeng-Longmaxi Formation shale in Well Y has not been severely fragmented and deformed. The results of pore structure characterization further show that OM pores are well preserved in tectonic deformation. However, Well M is located near the Jianshi fault zone in western Hubei. Due to the lack of rigid basement protection, most shale pores were destroyed during the tectonic movement.

5.3. Conceptual model for pore evolution

To clarify the response relationship between pore structure characteristics of shale and structural preservation conditions, we combined the tectonic geology background, shale fracture characteristics, and microscopic pore characteristics of shale in the study area and finally established the conceptual model for pore evolution under different tectonic preservation conditions (Fig. 15). As seen from the shale pore evolution model of Well Y (Model Y), Well Y is far from the regional tensile fault zone and less affected by fault

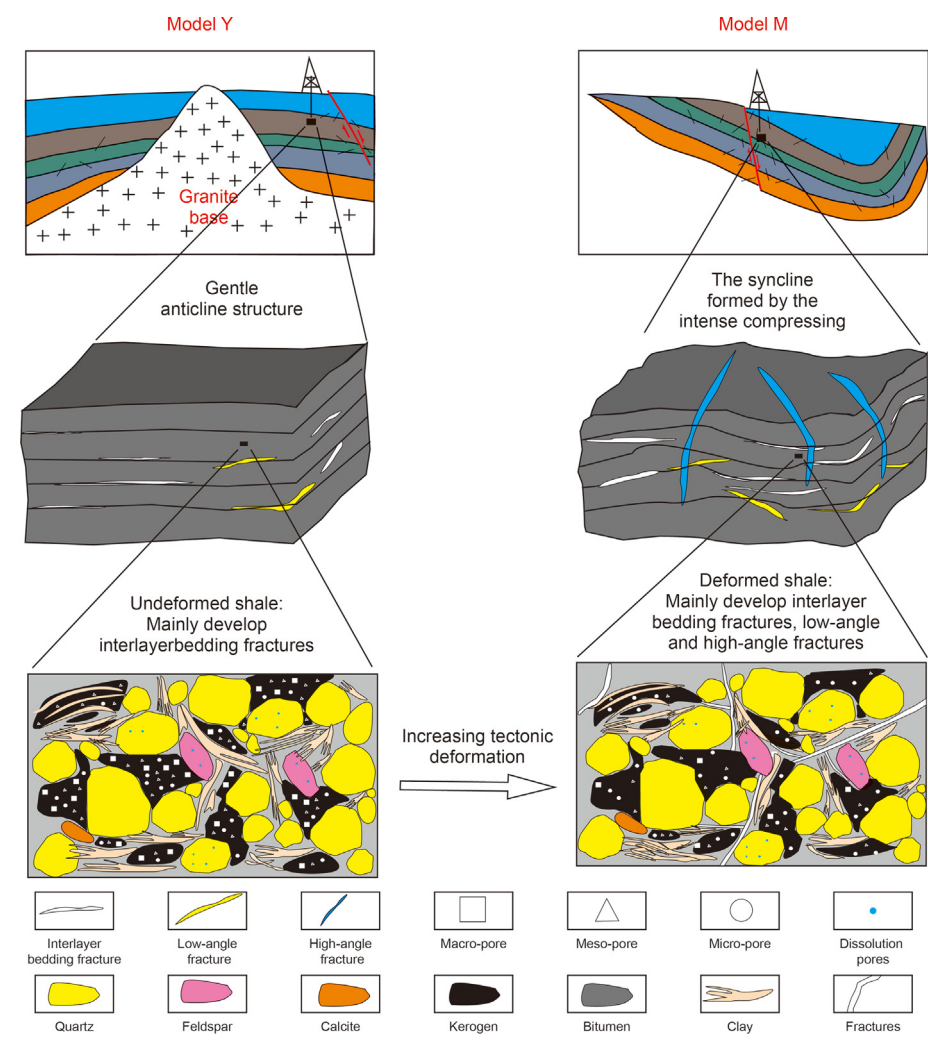


Fig. 15. The conceptual model for pore evolution of shale under different tectonic preservation conditions.

activity. Moreover, the rigid basement of the Huangling uplift has a certain anti-deformation effect on the overall structure of the region, which can resist the destruction of pores by the tectonic movement to a certain extent (Zhang et al., 2019; Chen et al., 2020). The cores show local fragmentation with a small number of bedding and low-angle fractures, which do not seriously damage the formation seal. Most pores are preserved by the support of the over-pressured fluid under compaction. Therefore, the statistical results of electron microscopy show that OM pores in stabilized shale have the advantages of high surface porosity, large size and good roundness. Furthermore, the shale in the stabilized zone has high porosity and pore volume. It can be believed that good tectonic preservation conditions are conducive to the preservation of OM pores.

As shown in Model M, a series of medium-high angle shear fractures are developed in the deformed shales under the influence of fault movement. In addition, under formation uplift and denudation, some closed fractures will be reopened due to changes in formation pressure. These fractures interweave and connect to form a good channel for natural gas to escape, resulting in poor sealing conditions of shale reservoirs. OM pores that have lost the support of over-pressure fluid collapsed and closed under compaction, decreasing the porosity and pore volume significantly. Generally, poor tectonic preservation conditions are not conducive to the preservation of shale pores.

5.4. Implications for shale gas exploration in complex tectonic zones

Compared with the shale reservoirs in North America, the shales in China's southern marine complex tectonic zones have undergone multiple phases of tectonic movements, resulting in highly complex tectonic preservation conditions and reservoir characteristics. Previous studies have found that tectonic preservation condition is the key to controlling pore development and shale gas enrichment (Sun et al., 2020; Gou et al., 2021a; Feng et al., 2022). Tectonic factors affecting preservation conditions include fracturing and uplift denudation. Since the late Yanshan period, the large-scale fracture activities occurring in the peripheral area of the Sichuan Basin have been intensifying, and the depth of fracture cutting commonly reaches 3 km (Shi et al., 2022). Moreover, the shale in the complex tectonic zone around the Sichuan Basin has experienced strong tectonic uplift. The uplift and denudation lead to brittle rupture due to the change of stratigraphic stress state, making the formed cracks in the reopening state or even leading to the destruction of the cover closure conditions. Eventually, the effective pore space in the shale is rapidly reduced under the action of factors such as the release of pressure from the formation, the release of fluids, and the pressure of the overlying strata (Xu et al., 2020b; Gou et al., 2021a). It is worth noting that tectonic uplift with ancient rigid basements like the Huangling uplift has the effect of

heat preservation and deformation resistance, which is favorable to the preservation of pores and the enrichment of shale gas. Therefore, we should prioritize the tectonic stability zones around the uplift with rigid basements or with the characteristics of being far away from the fracture zones, late and slow uplift, deep burial, etc., as favorable exploration areas for shale gas. Xu et al. (2020b) also pointed out that the gas content of the shale in the two wings of the Jiaoshiba (tectonic deformation area) is significantly lower than the shale in the main part of the Jiaoshiba (tectonic stability area). Therefore, for the southern marine shales that have experienced strong tectonic deformation, it is important to look for areas with relatively low weak tectonic deformation area (Gou et al., 2021a; c).

6. Conclusions

- (1) The average TOC content of shale samples in Well Y and Well M in the study area is 2.30% and 2.93%, and the thermal maturity is 2.05% and 2.56%, respectively. In addition, the mineral composition of the two wells shales is similar, mainly quartz and clay. The high TOC content, moderate thermal evolution degree, and more brittle minerals indicate that the two wells shales have good pores-generating capacity and pores-supporting capacity.
- (2) Compared with the stable zone, the porosity, pore volume, and specific surface area of the deformation zone are also reduced by 60.61%, 64.85%, and 27.81%, respectively, and the macro-pores and meso-pores are significantly reduced by 54.01% and 84.95%, respectively. Tectonic activity mainly leads to the compression and collapse of pores and macro-scopic pores in shale, so the influence on pore volume is greater than that on the relative surface area. The tectonic preservation condition is the main reason that controls the difference of pore structure of Wufeng-Longmaxi Formation shale in the study area. Fault activity and uplift denudation can cause collapse closure of pores without over-pressurized fluid support. The rigid basement of the Huangling uplift has the function of heat preservation and deformation resistance, which is conducive to preserving pores.
- (3) Based on the tectonic characteristics, core characteristics, and microscopic pore structure of shale reservoirs in the study area, a conceptual model of the pore evolution process of the Wufeng-Longmaxi Formation shale gas reservoirs in western Hubei under different tectonic preservation conditions was established. The differences in pore structure characteristics of shale under different tectonic preservation conditions were described, and the controlling effect of structural preservation conditions on pore evolution was illustrated.

Declaration of competing interest

The authors declare that they have no known competing financial interests or personal relationships that could have appeared to influence the work reported in this paper.

Acknowledgements

This research was supported by the National Natural Science Foundation of China (42122017, 41821002), the Hubei Provincial Natural Science Foundation of China (2020CFB501), the Shandong Provincial Key Research and Development Program (2020ZLYS08), and the Independent innovation research program of China University of Petroleum (East China) (21CX06001A).

References

- Bao, S.J., Zhai, G.Y., Zhou, Z., Yu, S.F., Chen, K., Wang, Y.F., Wang, H., Liu, Y.M., 2018. The evolution of the Huangling uplift and its control on the accumulation and preservation of shale gas. China Geol 1 (3), 346–353. https://doi.org/10.31035/ cg2018052
- Cai, Q.S., Chen, X.H., Zhang, G.T., Zhang, B.M., Han, J., Chen, L., Li, P.J., Li, Y.G., 2021. Shale gas reservoir development characteristics and exploration potential of Lower Paleozoic Wufeng Formation-Longmaxi Formation in Yichang area, western Hubei. Oil Gas Geol. 42 (1), 107–123. https://doi.org/10.11743/ ogg20210110 (in Chinese).
- Cai, Q.S., Hu, M.Y., Zhang, B.M., Ngia, N., Liu, A., Liao, R.Q., Kane, O., Li, H., Hu, Z.G., Deng, Q.J., Shen, J.J., 2022. Source of silica and its implications for organic matter enrichment in the Upper Ordovician-Lower Silurian black shale in western Hubei Province, China: Insights from geochemical and petrological analysis. Petrol. Sci. 19 (1), 74–90. https://doi.org/10.1016/j.petsci.2021.10.012.
- Cao, T.T., Deng, M., Song, Z.G., Luo, H.Y., Hursthouse, A.S., 2018. Characteristics and controlling factors of pore structure of the Permian shale in southern Anhui province, East China. J. Nat. Gas Sci. Eng. 60, 228–245. https://doi.org/10.1016/ i.ingse.2018.10.018.
- Chalmers, G.R., Bustin, R.M., Power, I.M., 2012. Characterization of gas shale pore systems by porosimetry, pycnometry, surface area, and field emission scanning electron microscopy/transmission electron microscopy image analyses: examples from theBarnett, Woodford, Haynesville, Marcellus, and Doig unit. AAPG Bull. 96 (6), 1099–1119. https://doi.org/10.1306/10171111052.
- Chen, J., Xiao, X., 2014. Evolution of nanoporosity in organic-rich shales during thermal maturation. Fuel 129, 173—181. https://doi.org/10.1016/j.fuel.2014.03.058.
- Chen, K., Zhai, G.Y., Bao, S.J., Song, T., Lin, T., Li, H.H., Jin, C.S., Meng, F.Y., Tang, X.C., Zhang, Y.L., 2020. Structural evolution of the Huangling uplift in South China and its control on shale gas preservation. China Geol 47 (1), 161–172. https:// doi.org/10.12029/gc20200113 (in Chinese).
- Dong, T., He, S., Chen, M.F., Hou, Y.G., Guo, X.W., Wei, C., Han, Y.J., Yang, R., 2019. Quartz types and origins in the paleozoic Wufeng-Longmaxi Formations, Eastern Sichuan Basin, China: implications for porosity preservation in shale reservoirs. Mar. Petrol. Geol. 106, 62–73. https://doi.org/10.1016/ i.marpetgeo.2019.05.002.
- Feng, Q.Q., Qiu, N.S., Borjigin, T., Wu, H., Zhang, J.T., Shen, B.J., Wang, J.S., 2022. Tectonic evolution revealed by thermo-kinematic and its effect on shale gas preservation. Energy 240, 122781. https://doi.org/10.1016/j.energy.2021.122781.
- Furmann, A., Mastalerz, M., Schimmelmann, A., Pedersen, P.K., Bish, D., 2014. Relationships between porosity, organic matter, and mineral matter in mature organic-rich marine mudstones of the Belle Fourche and Second White Specks formations in Alberta, Canada. Mar. Petrol. Geol. 54, 65–81. https://doi.org/10.1016/j.marpetseo.2014.02.020.
- Gao, Z.Y., Fan, Y.P., Xuan, Q.X., Zheng, G.W., 2020. A review of shale pore structure evolution characteristics with increasing thermal maturities. Adv. Geo-Energy Res. 4 (3), 247–259. https://doi.org/10.46690/ager.2020.03.03.
- Ge, X., Shen, C.B., Yang, Z., Mei, L.F., Xu, S.H., Peng, L., Liu, Z.Q., 2013. Low-temperature thermochronology constraints on the mesozoic-cenozoic exhumation of the Huangling massif in the Middle Yangtze Block, Central China. J. Earth Sci. 24, 541–552. https://doi.org/10.1007/s12583-013-0348-8.
- Gou, Q.Y., Xu, S., Hao, F., Yang, F., Zhang, B.Q., Shu, Z.G., Zhang, A.H., Wang, Y.X., Lu, Y.B., Cheng, X., Qing, J.W., Gao, M.T., 2019. Full-scale pores and microfractures characterization using FE-SEM, gas adsorption, nano-CT and micro-CT: a case study of the Silurian Longmaxi Formation shale in the Fuling area, Sichuan Basin, China. Fuel 253, 167–179. https://doi.org/10.1016/j.fuel.2019.04.116.
- Gou, Q.Y., Xu, S., Hao, F., Yang, F., Shu, Z.G., Liu, R., 2021a. The effect of tectonic deformation and preservation condition on the shale pore structure using adsorption-based textural quantification and 3D image observation. Energy 219, 119579. https://doi.org/10.1016/j.energy.2020.119579.
- Gou, Q.Y., Xu, S., Hao, F., Shu, Z.G., Zhang, Z.Y., 2021b. Making sense of microfractures to the Longmaxi shale reservoir quality in the Jiaoshiba area, Sichuan Basin, China: implications for the accumulation of shale gas. J. Nat. Gas Sci. Eng. 94, 104107. https://doi.org/10.1016/j.jngse.2021.104107.
- Gou, Q.Y., Xu, S., Hao, F., Lu, Y.B., Shu, Z.G., Lu, Y.C., Wang, Z.K., Wang, Y.F., 2021c. Evaluation of the exploration prospect and risk of marine gas shale, southern China: a case study of Wufeng-Longmaxi shales in the Jiaoshiba area and Niutitang shales in the Cen'gong area. GSA Bull. 134 (5–6), 1585–1602. https://doi.org/10.1130/b36063.1.
- Guo, X.C., Liu, R., Xu, S., Feng, B., Wen, T., Zhang, T.S., 2022. Structural deformation of shale pores in the fold-thrust belt: the Wufeng-Longmaxi shale in the Anchang syncline of Central Yangtze Block. Adv. Geo-Energy Res. 6 (6), 515–530. https://doi.org/10.46690/ager.2022.06.08.
- He, Z.L., Nie, H.K., Zhang, Y.Y., 2016. Analysis on main controlling factors of shale gas enrichment in Ordovician Wufeng Formation and Silurian Longmaxi Formation, Sichuan Basin and its periphery. Geosci. Front. 23 (2), 817. https://doi.org/ 10.13745/j.esf.2016.02.002 (in Chinese).
- Hu, D.F., Zhang, H.R., Ni, K., Yu, G.C., 2014. Preservation conditions for marine shale gas at the southeastern margin of the Sichuan Basin and their controlling factors. Nat. Gas Industry. B. 1 (2), 178–184. https://doi.org/10.1016/ i.ngib.2014.11.009.
- Hu, G., Pang, Q., Jiao, K., Hu, C.W., Liao, Z.W., 2020. Development of organic pores in

the Longmaxi Formation overmature shales: combined effects of thermal maturity and organic matter composition. Mar. Petrol. Geol. 116, 104314. https://doi.org/10.1016/j.marpetgeo.2020.104314.

- Jiao, L., Andersen, P.Ø., Ping, Z.J., Cai, J., 2020. Applications of mercury intrusion capillary pressure for pore structures: a review. Capillarity 3 (4), 62–74. https://doi.org/10.46690/capi.2020.04.02.
- Liang, M.L., Wang, Z.X., Gao, L., Li, C.L., Li, H.J., 2017. Evolution of pore structure in gas shale related to structural deformation. Fuel 197, 310—319. https://doi.org/10.1016/i.fuel.2017.02.035.
- Liu, S.G., Ye, Y.H., Ran, B., Jiang, L., LI, Z.W., Li, J.X., Song, J.M., Jiao, K., Li, Z.Q., Li, Y.W., 2020. Evolution of shale pore structure characteristics under different preservation conditions and significance. Journal of Reservoir Evaluation and Development 10 (5), 1-11 (in chinese) doi: https://doi.org/10.13809/j.cnki.cn32-1825/ te 2020 05 001
- Liu, Y.S., Jin, J.N., Pan, R.F., Li, X.T., Zhu, Z.P., 2023. Evaluation of atmospheric shale gas preservation conditions of Wufeng-Longmaxi Formation in the basin margin transition zone of southeast Chongqing. Bulletin of Geological Science and Technology 42 (1), 253–263. https://doi.org/10.19509/j.cnki.dzkq.tb20210768 (in Chinese).
- Milliken, K.L., Esch, W., Reed, R., Zhang, T.W., 2012. Grain assemblages and strong diagenetic overprinting in siliceous mudrocks, Barnett shale (Mississippian), Fort Worth basin, Texas. AAPG Bull. 96 (8), 1553—1578. https://doi.org/10.1306/12011111129
- Milliken, K.L., Rudnicki, M., Awwiller, D.N., Zhang, T.W., 2013. Organic matter-hosted pore system, Marcellus formation (Devonian), Pennsylvania. AAPG Bull. 97, 177–200. https://doi.org/10.1306/07231212048.
- Mastalerz, M., Schimmelmann, A., Drobniak, A., Chen, Y.Y., 2013. Porosity of Devonian and Mississippian New Albany Shale across a maturation gradient: Insights from organic petrology, gas adsorption, and mercury intrusion. AAPG Bull. 97 (10), 1621—1643. https://doi.org/10.1306/04011312194.
 Ma, Y., Ardakani, O.H., Zhong, N.N., Liu, H.L., Huang, H.P., Larter, S., Zhang, C., 2020.
- Ma, Y., Ardakani, O.H., Zhong, N.N., Liu, H.L., Huang, H.P., Larter, S., Zhang, C., 2020. Possible pore structure deformation effects on the shale gas enrichment: an example from the Lower Cambrian shales of the Eastern Upper Yangtze Platform, South China. Int. J. Coal Geol. 217, 103349. https://doi.org/10.1016/j.coal.2019.103349.
- Ross, D.J.K., Bustin, R.M., 2009. The importance of shale composition and pore structure upon gas storage potential of shale gas reservoirs. Mar. Petrol. Geol. 26 (6), 916–927. https://doi.org/10.1016/j.marpetgeo.2008.06.004.
- Slatt, R.M., O'Brien, N.M., 2009. Pore types in the Barnett and Woodford gas shales: contribution to understanding gas storage and migration pathways in finegrained rocks. AAPG Bull. 95 (12), 2017–2030. https://doi.org/10.1306/ 03301110145
- Shi, Y.G., Tang, X.L., Wu, W., Jiang, Z.X., Xiang, S.Q., Wang, M., Zhou, Y.R., Xiao, Y.P., 2022. Control of complex structural deformation and fractures on shale gas enrichment in southern Sichuan Basin, China. Energy & Fuels 36 (12), 6229–6242. https://doi.org/10.1021/acs.energyfuels.2c00993.
- Si, C.Y., Tan, J.Q., Wang, Z.H., Ma, X., 2022. Characteristics and influencing factors of shale pore development in Niutitang Formation of Cambrian, western Hunan. J. Cent. S. Univ. 53 (9), 3738–3755. https://doi.org/10.11817/j.issn.1672-7207.2022.09.034 (in Chinese).
- Sun, W.J.B., Zuo, Y.J., Lin, Z., Wu, Z.H., Liu, H., Lin, J.Y., Chen, B., Chen, Q.G., Pan, C., Lan, B.F., Liu, S., 2023. Impact of tectonic deformation on shale pore structure using adsorption experiments and 3D digital core observation: a case study of the Niutitang Formation in Northern Guizhou. Energy 278, 127724. https://doi.org/10.1016/j.energy.2023.127724.
- Sun, W.J.B., Zuo, Y.J., Wang, S.Y., Wu, Z.H., Liu, H., Zheng, L.J., Lou, Y.L., 2020. Pore structures of shale cores in different tectonic locations in the complex tectonic region: a case study of the Niutitang Formation in Northern Guizhou, Southwest China. J. Nat. Gas Sci. Eng. 80, 103398. https://doi.org/10.1016/j.jngse.2020.103398.
- Teng, J., Liu, B., Mastalerz, M., Schieber, J., 2022. Origin of organic matter and organic pores in the overmature Ordovician-Silurian Wufeng-Longmaxi shale of the Sichuan Basin, China. Int. J. Coal Geol. 253, 103970. https://doi.org/10.1016/ i.coal.2022.103970.
- Wang, G.C., 2020. Deformation of organic matter and its effect on pores in mudrocks. AAPG Bull. 104 (1), 21–36. https://doi.org/10.1306/04241918098.
- Wang, J.Y., Guo, S.B., 2021. Study on the relationship between hydrocarbon generation and pore evolution in continental shale from the Ordos Basin, China. Petrol. Sci. 18 (5), 18. https://doi.org/10.1016/j.petsci.2021.01.002.
- Wang, R.Y., Hu, Z.Q., Zhou, T., Bao, H.Y., Wu, J., Du, W., He, J.H., 2021a. Shale fracture development characteristics and reservoir control significance of Wufeng-Longmaxi Formation in Sichuan Basin and its periphery. Oil Gas Geol. 42 (6), 1295—1306. https://doi.org/10.11743/ogg20210605 (in Chinese).
- Wang, Y., Dong, D., Cheng, X., Huang, J.L., Wang, S.F., Wang, S.Q., 2014. Electric property evidences of carbonification of organic matters in marine shales and its geologic significance: a case study of the Lower Cambrian Qiongzhusi shale in the southern Sichuan Basin. Nat. Gas Industry. B. 1 (2), 129–136. https:// doi.org/10.1016/j.ngib.2014.11.002.

- Wang, Y., Liu, L.F., Cheng, H.F., 2021b. Gas adsorption characterization of pore structure of organic-rich shale: Insights into contribution of organic matter to shale pore network. Nat. Resour Res. 30, 2377–2395. https://doi.org/10.1007/ s11053-021-09817-5.
- Wei, S., He, S., Pan, Z.J., Guo, X.W., Yang, R., Dong, T., Yang, W., Gao, J., 2019. Models of shale gas storage capacity during burial and uplift: Application to Wufeng-Longmaxi shales in the Fuling shale gas field. Mar. Petrol. Geol. 109, 233–244. https://doi.org/10.1016/j.marpetgeo.2019.06.012.
- Wu, L.Y., Hu, D.F., Lu, Y.C., Liu, R.B., Liu, X.F., 2016. Advantageous shale lithofacies of Wufeng Formation-Longmaxi Formation in fuling gas field of Sichuan Basin, SW China. Petrol. Explor. Dev. 43 (2), 208–217. https://doi.org/10.1016/s1876-3804(16)30024-6.
- Xi, Z.D., Tang, S.H., Li, J., Zhang, Z.Y., Xiao, H.Q., 2019. Pore characterization and the controls of organic matter and quartz on pore structure: case study of the Niutitang Formation of northern Guizhou Province, South China. J. Nat. Gas Sci. Eng. 61, 18—31. https://doi.org/10.1016/j.jngse.2018.11.001.
- Xu, L.L., Wen, Y.R., Zhang, Y.L., Ren, Z.J., Yang, J., Wen, J.H., Chen, W., Luo, F., Duan, K., 2021. Gas-bearing characteristics and preservation conditions of upper Ordovician Wufeng FormationFormation-Lower Silurian Longmaxi Formation shale in western Hubei. Petroleum Geology. & Experiment 43 (3), 395–405. https://doi.org/10.11781/sysydz202103395 (in Chinese).
- Xu, S., Hao, F., Shu, Z.G., Zhang, A.H., Yang, F., 2020a. Pore structures of different types of shales and shale gas exploration of the Ordovician Wufeng and Silurian Longmaxi successions in the eastern Sichuan Basin, South China. J. Asian Earth Sci. 193. 104271. https://doi.org/10.1016/j.iseaes.2020.104271.
- Sci. 193, 104271. https://doi.org/10.1016/j.jseaes.2020.104271.

 Xu, S., Gou, Q.Y., Hao, F., Zhang, B.Q., Shu, Z.G., Lu, Y.B., Wang, Y.X., 2020b. Shale pore structure characteristics of the high and low productivity wells, Jiaoshiba shale gas field, Sichuan Basin, China: dominated by lithofacies or preservation condition? Mar. Petrol. Geol. 114, 104211. https://doi.org/10.1016/j.marpetgeo.2019.104211.
- Yang, W., Wang, Y.H., Du, W., Song, Y., Jiang, Z.X., Wang, Q.Y., Xu, L., Zhao, F.P., Chen, Y., Shi, F.L., Yao, S.H., Hou, H.D., Xiong, S.L., 2022. Behavior of organic matter-hosted pores within shale gas reservoirs in response to differential tectonic deformation: potential mechanisms and innovative conceptual models. J. Nat. Gas Sci. Eng. 102, 104571. https://doi.org/10.1016/j.jngse.2022.104571.
- Yasin, Q., Sohail, G.M., Liu, K.Y., Du, Q.Z., Boateng, C.D., 2021. Study on brittleness templates for shale gas reservoirs-A case study of Longmaxi shale in Sichuan Basin, southern China. Petrol. Sci. 18 (5), 20. https://doi.org/10.1016/ i.petsci.2021.09.030.
- Yuan, Y.S., Jin, Z.J., Zhou, Y., Liu, J.X., Li, S.J., Liu, Q.Y., 2017. Burial depth interval of the shale brittle-ductile transition zone and its implications in shale gas exploration and production. Petrol. Sci. 14 (4), 11. https://doi.org/10.1007/s12182-017-0189-7
- Zhai, G.Y., Bao, S.J., Pang, F., Ren, S.M., Chen, K., Wang, Y.F., Zhou, Z., Wang, S.J., 2017. Study on hydrocarbon accumulation model of four-story shale in Anchang syncline, Zunyi area, Guizhou. China Geol 44 (1), 1–12. https://doi.org/10.12029/srs20170.101
- Zhai, G.Y., Wang, Y.F., Liu, G.H., Zhou, Z., Bao, S.J., Chen, K., Kang, H., Zhang, J.Z., Wang, S.J., Zhang, Y.X., 2019. The Sinian-Cambrian formation shale gas exploration and practice in southern margin of Huangling paleo-uplift. Mar. Petrol. Geol. 109, 419–433. https://doi.org/10.1016/j.marpetgeo.2019.06.036.
- Zhang, J.F., Xu, H., Zhou, Z., Ren, P.F., Guo, J.Z., Wang, Q., 2019. Geological characteristics of shale gas accumulation in Yichang area of western Hubei. Acta Petrol. Sin. 40 (8), 887–899. https://doi.org/10.7623/syxb201908001 (in Chinese).
- Zhang, Y.F., Yu, B.S., Pan, Z.J., Hou, C.H., Zuo, Q.W., Sun, M.D., 2020. Effect of thermal maturity on shale pore structure: a combined study using extracted organic matter and bulk shale from Sichuan Basin, China. J. Nat. Gas Sci. Eng. 74, 103089. https://doi.org/10.1016/j.jngse.2019.103089.
- Zhang, B.M., Cai, Q.S., Chen, X.H., Wang, C.S., Zhang, G.T., Chen, L., LI, P.J., Li, Y.G., 2021. Shale gas reservoir characteristics and gas bearing capacity of Wufeng-Longmaxi Formation in Well Eyiye 2, eastern margin of Huangling Uplift, western Hubei. China Geol. 48(05), 1485-1498 (in chinese) doi: https://doi.org/10.12029/gc20210513.
- Zhao, J.H., Jin, Z.J., Hu, Q.H., Hu, Q.H., Liu, K.Y., Jin, Z.K., Hu, Z.Q., Nie, H.K., Du, W., Yan, C.N., Wang, R.Y., 2018. Mineral composition and seal condition implicated in pore structure development of organic-rich Longmaxi shales, Sichuan Basin, China. Mar. Petrol. Geol. 98, 507–522. https://doi.org/10.1016/j.marpetgeo.2018.09.009.
- Zhou, Z., Jiang, Z.X., Li, S.Z., Xu, G.H., Wang, S.J., Gou, T.X., Tong, C.C., 2021. Biostratigraphic characteristics of black shale in Wufeng-Longmaxi Formation, Jianshi area, western Hubei. Earth Sci. 46 (2), 432–443. https://doi.org/10.3799/dqkx.2020.059 (in Chinese).
- Zhu, H.J., Ju, Y.W., Qi, Y., Huang, C., Zhang, L., 2018. Impact of tectonism on pore type and pore structure evolution in organic-rich shale: implications for gas storage and migration pathways in naturally deformed rocks. Fuel 228, 272–289. https://doi.org/10.1016/j.fuel.2018.04.137.